Detecting dark matter annihilation with CMB polarization: Signatures and experimental prospects

Citation
Padmanabhan, Nikhil, and Douglas P. Finkbeiner. 2005. "Detecting Dark Matter Annihilation with CMB Polarization: Signatures and Experimental Prospects." Physical Review D 72 (2) (July 12). doi:10.1103/physrevd.72.023508.

Published Version
10.1103/physrevd.72.023508

Permanent link
http://nrs.harvard.edu/urn-3:HUL.InstRepos:33461881

Terms of Use

Share Your Story

The Harvard community has made this article openly available.
Please share how this access benefits you. Submit a story .

Accessibility

Detecting Dark Matter Annihilation with CMB Polarization : Signatures and Experimental Prospects

Nikhil Padmanabhan[1, *] and Douglas P. Finkbeiner[2, †]

^{1}Joseph Henry Laboratories, Jadwin Hall, Princeton University, Princeton, NJ 08544, USA

^{2}Dept. of Astrophysical Sciences, Peyton Hall, Princeton University, Princeton, NJ 08544, USA

(Dated: February 2, 2008)

Dark matter (DM) annihilation during hydrogen recombination ($z \sim 1000$) will alter the recombination history of the Universe, and affect the observed CMB temperature and polarization fluctuations. Unlike other astrophysical probes of DM, this is free of the significant uncertainties in modelling galactic physics, and provides a method to detect and constrain the cosmological abundances of these particles. We parametrize the effect of DM annihilation as an injection of ionizing energy at a rate ϵ_{dm}, and argue that this simple "on the spot" modification is a good approximation to the complicated interaction of the annihilation products with the photon-electron plasma. Generic models of DM do not change the redshift of recombination, but change the residual ionization after recombination. This broadens the surface of last scattering, suppressing the temperature fluctuations and enhancing the polarization fluctuations. We use the temperature and polarization angular power spectra to measure these deviations from the standard recombination history, and therefore, indirectly probe DM annihilation. The modifications to the temperature power spectrum are nearly degenerate with the primordial scalar spectral index and amplitude; current CMB data are therefore unable to put any constraints on the annihilation power. This degeneracy is broken by polarization; *Planck* will have the sensitivity to measure annihilation power $\epsilon_{dm}(z = 1000) > 10^{-15}$ eV/s/proton, while high sensitivity experiments (eg. NASA's CMBPOL) could improve that constraint to $\epsilon_{dm}(z = 1000) > 4 \times 10^{-16}$ eV/s/proton, assuming a fractional detector sensitivity of $\Delta T/T \sim 1\mu$K and a beam of $3'$. These limits translate into a lower bound on the mass of the DM particle, $M_{dm} > 10 - 100$ GeV, assuming a single species with a cross section of $\langle \sigma_A v \rangle \sim 2 \times 10^{-26}$ cm^3/s, and a fraction $f \sim 0.1 - 1$ of the rest mass energy used for ionization. The bounds for the *WMAP* 4y data are significantly lower, because of its lack of high S/N polarization measurements, but it can strongly constrain $\mathcal{O}($ MeV$)$ particles such as those proposed by Boehm et al (2004).

PACS numbers:

I. INTRODUCTION

There is a broad consensus that the majority of the matter in the universe is non-luminous, non-baryonic "dark matter" (DM) [see 1, 2, for recent reviews]. Some of the first compelling evidence for DM came from galaxy rotation curves, suggesting that a large fraction of the mass lay beyond the luminous extent of the galaxy. Similar conclusions were reached for massive clusters of galaxies using the gravitational distortion of the images of background galaxies. Measurements of the deuterium abundance, combined with big-bang nucleosynthesis indicate that density of baryons is less than the estimated mass density. This is supported by measurements of the temperature fluctuations of the cosmic microwave background (CMB) radiation made by the *WMAP* satellite[3]. Dark matter is an integral part of the cosmological "standard model", constituting 80% of the total matter in the Universe.

Cosmology also constrains the gravitational properties of the DM. The spatial clustering of galaxies and the angular power spectrum of CMB temperature fluctuations strongly favor a non-relativistic pressureless species for the DM, while N-body simulations show that this clustering is consistent with the DM being composed of weakly interacting particles whose dominant long-range interactions are gravitational. This suggests that the DM particle is a weakly interacting massive particle (WIMP), although more exotic possibilities are not ruled out. We, however, will focus solely on WIMPs for this paper.

A theoretical description of the DM is still unknown, although it is believed that such a description involves physics beyond the Standard Model. There are strong theoretical reasons for believing that the Standard Model is modified at the electroweak symmetry scale ~ 1 TeV, intriguingly the same energy scale for WIMPs predicted by the present mass density. These modifications range from supersymmetric extensions of the Standard Model to large extra dimensions modifying gravity on these scales, and generically have a zoo of massive particles with properties that make them potential DM candidates. The relevant energies are just entering the reach of current direct detection experiments[4] and accelerator energies, and will be strongly constrained by the next generation of these experiments.

While there is no substitute for a direct detection of

WIMPs, astrophysical probes of DM play an important role, since they provide a complementary view of the DM parameter space, making different assumptions than particle physics experiments. Furthermore, probing the cosmological abundance of a candidate particle requires an astrophysical probe. There already are a few tantalizing observations suggesting a DM particle between $\sim 1 - 100$ GeV. The γ-ray emission measured by the EGRET instrument on the *Compton Gamma Ray Observatory* has a higher amplitude at $\gtrsim 1$ GeV than traditional models of the Galactic cosmic ray population and interstellar medium models allow [5, 6, 7]. The $e^\pm$ annihilation line strength at 511 keV observed by Integral/SPI suggests a surprising Galaxy-wide positron production rate of 10^{44} s^{-1} [8]. Furthermore, the cosmic-ray positron ratio observed by HEAT shows an excess above 5 GeV consistent with simple models of Higgsino decay [9]. The synchrotron haze in the inner Milky Way [10] may be an example of synchrotron emission from $e^\pm$ pairs produced by ongoing DM annihilations as suggested by [11]. The observed synchrotron signal could be produced by a fiducial model of 100 GeV particles annihilating at $\langle \sigma_A v \rangle = 2 \times 10^{-26}$ cm^3 s^{-1} and distributed with an NFW[12] mass profile[13]. This model is not expected to be correct in detail, but is a fiducial model scalable to other possible scenarios.

In this paper, we propose using the CMB temperature and polarization fluctuations as a probe of DM annihilation. DM annihilation at $z \sim 1000$ injects energy into the photon-baryon plasma ionizing neutral hydrogen and modifies the recombination history. These additional electrons scatter CMB photons, making the last scattering surface thicker and attenuating correlations between temperature perturbations. On the other hand, the correlations between polarization fluctuations are enhanced by the thicker scattering surface. This alters the temperature and polarization angular power spectra, providing a handle on the properties of the DM. The CMB has an important advantage over the other probes discussed above, as computing the power spectrum is a linear calculation based on well understood physics. This enables detecting small deviations from the expected signal (that herald new physics) at a high level of significance. This should be contrasted with the other probes discussed above that require additional information such as the DM distribution and clumpiness, ISM density, magnetic field strength and degree of tangling, Galactic photon energy density etc., all of which are complex processes with significant uncertainties.

Modifications to the recombination history, ranging from delayed recombination to low redshift ionization from DM decays, and their effect of the CMB have been considered by [eg. 14, 15, 16, 17, 18, 19]. Most recently, these ideas have been used to attempt to explain the high optical depth observed by the *WMAP* satellite by using DM decays to reionize the universe. The goals of this paper significantly differ from such studies. We aim to understand how the CMB (via the recombination history) constrains the parameters of an annihilating DM model. Since we lack a preferred theoretical framework for the DM, we construct a generic parametrization of DM annihilation to effectively constrain the DM model space. We parametrize DM annihilation as an energy injection into the IGM[44] and relate this energy to standard parameters like the DM mass and annihilation cross section. Given a specific model of the DM, constraints on this injection energy can then be used to constrain the parameters of that model.

We start (Sec. II) by discussing the effect of DM annihilation on the ionization history of the Universe, introducing the "on the spot" approximation as a useful parametrization of the more complex processes responsible. Sec. III then discusses the effect of this change to the ionization history on the CMB, while Sec. IV attempts to quantify the detectability of these effects. Sec. V considers whether other astrophysical probes have the potential to probe DM annihilation during the recombination epoch, and Sec. VI summarizes the principal conclusions of this paper, and discusses their implications.

A note on cosmology and notation: if not explicitly specified, we will assume a concordance fiducial model with $\Omega_M + \Omega_\Lambda = 1$, $\Omega_M = 0.3$, $\Omega_b = 0.05$, $h = 0.7$, $Y_{He} = 0.24$ and $n_s = 1$. We only consider the scalar contributions to the CMB fluctuations, and therefore describe the temperature and polarization fluctuations by the temperature-temperature (TT), temperature-polarization (TE), and polarization-polarization (EE) power spectra. Finally, proper and comoving times are t and η respectively, while a 0 subscript denotes the present epoch.

II. THE IONIZATION HISTORY

The effect of DM annihilation on the recombination history can be conveniently, albeit artificially, separated into two stages – the injection of the energy from the annihilation into the IGM, and the effect of this energy on recombination. We argue that the former process is well approximated by a rate of energy injection per hydrogen atom (ϵ_{dm}), instantaneously used to ionize and heat the IGM. We then consider how this energy changes the ionization fraction as a function of time.

A. The "On the Spot" Approximation

How do DM annihilations cause ionizations? The primary products from an annihilation depend on the particular DM model, but generically are quarks, gauge bosons, leptons, and Higgs particles. These primaries tend to be unstable, and rapidly decay via hadronic-leptonic jets into showers of $e^\pm$ pairs, protons, photons and neutrinos. Given our ignorance about DM, we assume each annihilation partitions the majority of its energy between $e^\pm$ pairs, photons and neutrinos, whose en-
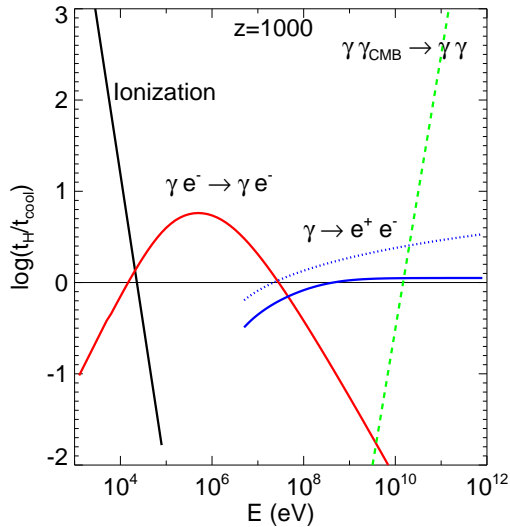
FIG. 1: A comparison of the photon cooling time to the Hubble time at $z = 1000$, for different photon energies. The dominant processes (in order of increasing energy) are ionization, Compton scattering, pair production, and photon-photon scattering. All the curves (except the dotted curve) assume a neutral IGM, with a density of 2×10^{-7} cm^{-3} atoms today. The dotted curve shows the pair production rate for a completely ionized IGM. Regions where $t_H/t_{cool} < 1$ are transparent; photons injected at these energies lose their energy by redshifting. Note that photon-photon scattering does not transfer the energy to electrons, but simply redistributes it to lower energies. This figure ignores pair production off CMB photons since this process is subdominant for the energy range considered here; it however dominates at higher energies.

ergy spectra can be calculated given the mass and couplings of the DM particle. Note that we are not assuming that these are directly produced by the annihilation, but simply that they are final products of the resulting particle cascades. The problem now simplifies to understanding the mechanisms by which $e^{\pm}$ pairs, photons and neutrinos inject energy into the IGM. Of these, neutrinos are the easiest to understand; they never interact and their energy is lost.

The interaction of photons with the IGM was considered in detail by [20] who find that the dominant processes (ordered by increasing photon energy) are photoionization, Compton scattering, pair production off nuclei and atoms, photon-photon scattering, and pair production off CMB photons (Fig. 1). To estimate the efficiency of these mechanisms, we compare the cooling time for each process, $t_{cool} \equiv 1/(d \ln E/dt)$, to the Hubble time, $t_H \equiv 1/H(z)$. Except for Compton scattering, we approximate the cooling time by the mean free time as most of the energy is lost in the first interaction. If $t_H \gg t_{cool}$ (Fig. 1), energy deposition is very efficient, either by directly ionizing the IGM, or by producing energetic electrons. Conversely, if $t_H \ll t_{cool}$, the universe

is optically thin and most of the energy is lost through the redshifting of photons and not to ionizations. The photon-photon scattering process [21] is an exception to the above - each scattering event, on average, equally divides the energy between the two photons. The photon energy spectrum therefore gets shifted to lower energies until either pair production starts to dominate, or the universe becomes transparent.

What happens to photons injected into the transparency window between $\sim 10^8 - 10^{10}$ GeV (Fig. 1)? The ratio $t_H/t_{cool} \propto (1+z)^{3/2}$ ($\propto (1+z)^{9/2}$ for two photon scattering), while the photon energy redshifts as $(1 + z)$. These photons therefore remain in the optically thin regime, and contribute to the diffuse photon background today (Sec. V).

The second component of energy injection comes from electrons [45], both from the annihilation products, as well as from Compton scattering and pair production considered above. Their energy loss has been considered by a number of authors [14, 22, 23]; we restrict ourselves to a brief discussion of the relevant processes and time scales. At high electron energies ($\gamma \gg 1$), the dominant energy loss is by inverse Compton scattering CMB photons. The cooling time is [22],

$$\left(\frac{1}{t_{cool}} \right) = \frac{-d \ln \gamma}{dt} = \frac{4\sigma_T c a_R T_{CMB}^4 \gamma}{3 m_e c^2} , \qquad (1)$$

where $T_{CMB} = 2.725(1+z)$K is the mean CMB temperature at the relevant redshift, a_R is the radiation constant, and $\sigma_T = 6.65 \times 10^{-25}$ cm^2 is the Thomson cross section. Comparing this to the Hubble time, one finds

$$\frac{t_H}{t_{cool}} \sim 10^5 \left(\frac{1+z}{1000} \right)^{5/2} \frac{1}{\sqrt{\Omega_M h^2}} \gamma , \qquad (2)$$

implying that inverse Compton cooling efficiently produces photons with energies

$$E_\gamma \sim 5 \left(\frac{1+z}{1000} \right) \left(\frac{E_e}{1 \text{ GeV}} \right)^2 \text{MeV} . \qquad (3)$$

Fig. 1 shows that electrons with energies < 100 MeV will produce photons that efficiently ionize hydrogen; above that energy, the scattered photons either produce an electromagnetic cascade by Compton scattering or pair production, or are scattered into the optically thin part of the spectrum from 10^8 to 10^{10} eV and escape.

At lower energies, the principal mechanisms for energy loss become collisional heating, excitations and ionizations[23]. At high kinetic energies, $E_e \gg 100$ eV, the cross section for collisional ionization is [23],

$$\sigma_{eH} = \frac{2.23 \times 10^{-15} \ln(E/13.6)}{E} \text{cm}^2 , \qquad (4)$$

(E measured in eV) implying $t_H/t_{cool} \gg 1$ at $z \sim 1000$. The results for collisions and excitations are very similar, although collisional losses become important at lower energies, 100 eV $< E < 1$ keV.
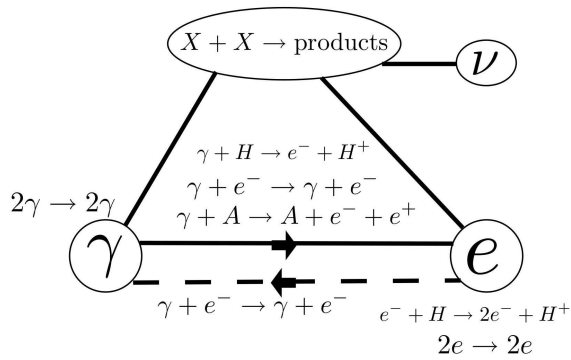
FIG. 2: The injection of energy from dark matter annihilation into the IGM, via the creation of electromagnetic cascades. Energy transfer to the IGM takes place principally through the ionization and collisional processes.

Our model of DM annihilation, summarized in Fig. 2, is

1. DM particles annihilate into jets, whose end products are dominated by electrons, photons and neutrinos.

2. The IGM is transparent to neutrinos; this energy is lost.

3. The photons and electrons trigger electromagnetic cascades, shifting their spectra to lower energies, until their energy is either deposited in the IGM, or is redshifted away when the photons enter an optically thin regime.

4. The time scales for the cascades and energy deposition are much smaller than the expansion time.

We parametrize the effect of DM annihilation by the rate of energy injection per hydrogen nucleus per time, ϵ_{dm}; furthermore, we assume this energy is instantaneously deposited into the IGM. This "on the spot" approximation has the virtue of being generic and independent of particular properties of the DM.

What is the magnitude and redshift dependence of ϵ_{dm}? Given a particle with mass M_{dm} and a thermally averaged cross-section $\langle \sigma_A v \rangle$, we obtain,

$$\epsilon_{dm} = f M_{dm} \left(\frac{\langle \sigma_A v \rangle n_{dm,0}^2}{n_{H,0}} \right) (1+z)^3 , \qquad (5)$$

where $n_{DM,0}$ and $n_{H,0}$ are the present densities of the dark matter and hydrogen particles respectively, and f is the fraction of the rest mass energy injected into the IGM. Assuming our fiducial cosmology with a single DM species, we find,

$$\epsilon_{dm} \sim f 10^{-24} (1+z)^3 \text{ eV s}^{-1}$$
$$\times \left[\left(\frac{100 \text{ GeV}}{M_{dm}} \right) \left(\frac{\langle \sigma_A v \rangle}{2 \times 10^{-26} \text{ cm}^3 \text{ s}^{-1}} \right) \right] . \qquad (6)$$

The injected energy is inversely proportional to the particle mass; more massive particles inject *less* energy into the IGM. We parametrize our ignorance of the annihilations and their effect on the IGM by a simple efficiency factor, f. Given a specific model, one can compute f and convert constraints on ϵ_{dm} into constraints on M_{dm} and other model parameters.

B. Recombination with DM annihilation

Given ϵ_{dm}, we compute its effect on the recombination history. This energy injection heats the IGM, and ionizes and excites the hydrogen and helium atoms. [23] compute the exact fractions converted to heat, ionization and excitation as a function of the ionization fraction, and find that for a neutral IGM, the energy is roughly equipartitioned between the three processes, while for a fully ionized plasma, all the energy is converted into heat. This suggests a simpler but adequate approximation [14] that $(1-x)/3$ of the energy goes into ionization and $(1+2x)/3$ into heating the IGM, where x is the ionization fraction and we assume that excitations neither change the matter temperature nor the ionization fraction.

We compute the recombination history using the public code RECFAST [24] modifying the evolution equations as follows,

$$-\delta \left(\frac{dx[H]}{dz} \right) =$$
$$\frac{\epsilon_{dm,0}}{13.6} \frac{1-x[H]}{3(1+f_{He})} \mathcal{F}(z) ,$$
$$-\delta \left(\frac{dx[He]}{dz} \right) =$$
$$\frac{\epsilon_{dm,0}}{24.6} \frac{1-x[He]}{3(1+f_{He})} \mathcal{F}(z) \qquad (7)$$

where $\epsilon_{dm,0}$ is the energy injection rate at the present epoch (in eV/s), and

$$\mathcal{F}(z) \equiv \frac{(1+z)^3}{H(z)(1+z)} . \qquad (8)$$

Additionally, the ionization fraction of a species A is defined as,

$$x[A] = \frac{n[A^+]}{n[A^+] + n[A]} , \qquad (9)$$

and f_{He} is the ratio of the number density of helium to that of hydrogen. The evolution of the matter temperature, T_m is similarly given by,

$$-\delta \left(\frac{dT_m}{dz} \right) =$$
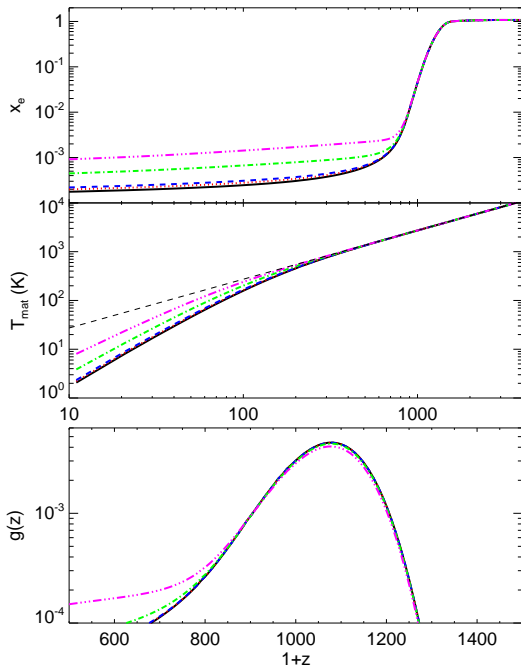$$\frac{2\epsilon_{dm,0}}{3k_B} \frac{1+2x[H]+f_{He}(1+2x[He])}{3(1+f_{He})} \mathcal{F}(z). \quad (10)$$

FIG. 3: The ionization fraction x_e (top), matter temperature (center), and visibility function (bottom) as a function of ϵ_{dm}. The heavy solid lines show the fiducial model with $\epsilon_{dm} = 0$; from bottom to top, $\epsilon_{dm,0} = 5, 10, 100, 500 \times 10^{-25}$ eV/s. The thin dashed line in the center plot shows the evolution of CMB temperature, $T(z) = T_0(1 + z)$. Note that the injection of additional energy does not slow recombination, but increases the residual ionization; this leaves the peak of the visibility function unchanged but broadens the surface of last scattering.

The resulting recombination and matter temperature histories for different values of $\epsilon_{dm,0}$ are shown in Fig. 3; the dominant effect is to change the residual ionization after recombination. This is easily explained by considering the competition between the recombination rate and the expansion of the universe. At early times, the recombination rate is significantly greater than the expansion rate and therefore, additional ionizations due to DM annihilation are immediately erased. As the recombination rate slows, these additional ionizations "freeze out", leading to a greater residual ionization fraction.

The evolution of the matter temperature is similar. At redshifts $\gg 100$, Compton scattering keeps the matter and radiation in tight thermal contact, and the excess energy from DM annihilation is lost in the extremely large heat capacity of the blackbody radiation. However, as the matter completely decouples from the radiation, annihilations start to increase the matter temperature, resulting in slower cooling relative to the fiducial model.

III. THE CMB AS A PROBE

Having computed the effect of DM annihilation on the recombination history, we attempt to understand its effect on the CMB. In what follows, it is sometimes convenient to parametrize the effect of DM annihilation by an ionization "floor" added to the standard recombination history. This lacks the physical intuition of ϵ_{dm}, but is a convenient analytic approximation. We define the optical depth to Thomson scattering,

$$\tau(\eta) = \int_\eta^{\eta_0} d\eta\, \sigma_T n_e c a \;, \tag{11}$$

where n_e is the free electron density. Assuming a matter dominated cosmology and constant ionization fraction x_e, this gives us

$$\tau(z) \sim 4 \times 10^{-2} x_e \frac{\Omega_b h(1 - Y_{He})}{\sqrt{\Omega_M}} z^{3/2} \;, \tag{12}$$

if $z \gg 1$.

A. Peak Positions

We begin by estimating the change in the position of the acoustic peaks in the temperature power spectrum due to an ionization floor. The probability that a photon last scattered between redshifts z and $z + dz$ is given by the visibility function,

$$g(z) \equiv \tau'(z) e^{-\tau(z)} \;, \tag{13}$$

shown in Fig. 3 for different recombination histories. The fraction of photons that scatter at a redshift $< z$, $G(z)$, is simply the integral of visibility function, $G(z) = 1 - \exp(-\tau(z))$. Since $g(z)$ is sharply peaked, we can meaningfully define a redshift of last scattering, z_{LS}, that determines the angular positions of the acoustic peaks. A convenient definition is $G(z_{LS}) = 0.5$ or $\tau(z_{LS}) \approx 0.7$ implying $z_{LS} \sim 1050$ for standard recombination. For the ionization floor to significantly shift the peaks, the additional optical depth, $\Delta\tau$, would have to be ~ 1. Using Eq. 12, this requires $10^3 x_{e,floor} \sim (\sqrt{\Omega_M}/\Omega_b h)$, or $x_{e,floor} \sim 0.01$ for our fiducial cosmology. As we shall see below, such an ionization fraction would have already noticeably affected the CMB temperature and polarization and therefore is strongly disfavored. More plausible values of the ionization floor do not noticeably shift the positions of the acoustic peaks in the temperature power spectrum.

B. Power Spectra

The effect of the altered recombination history on the CMB power spectra is discussed analytically below. However, the numerical results presented in the paper use
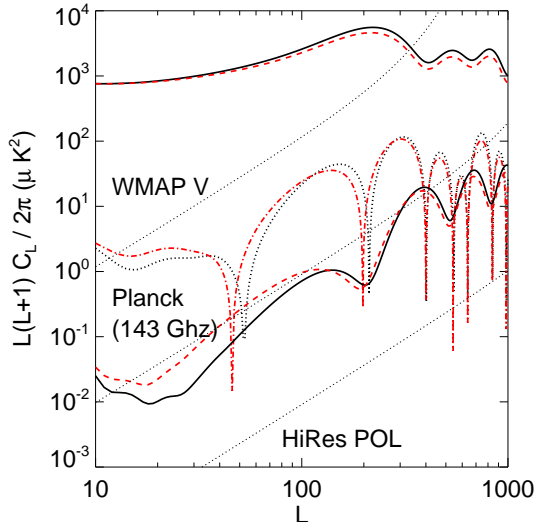
FIG. 4: The TT, TE, and EE angular power spectra for our fiducial cosmological model, with no DM annihilation (solid and dotted lines), and with $\epsilon_{dm,0} = 10^{-22}$ eV/s. Also shown are the polarization noise spectra, for the *WMAP* V band, the *Planck* 143 Ghz channel, and a hypothetical high resolution polarization experiment (see Table I for details).

the publicly available Boltzmann code `CAMB` [25], with the modified version of `RECFAST` described in the previous section, to obtain accurate power spectra. An example is shown in Fig. 4.

The temperature angular power spectrum is the photon distribution function convolved with the visibility function (the last scattering surface), and projected on the sky. The photon distribution function is unchanged by DM annihilation, but the visibility function extends to lower redshifts, broadening the surface of last scattering. This suppresses perturbations on scales smaller than the width of the surface, resulting in a relative attenuation of the power spectrum. This is scale dependent, with the largest scales attenuated the least and small scales the most. These effects are clearly seen in the accurate numerical solutions in Fig. 4.

Given the imminent high S/N temperature measurements due from the *WMAP* and *Planck* satellites, an immediate question is whether DM annihilation is detectable just using the temperature power spectrum. Unfortunately, the effects of ϵ_{dm} described above are almost perfectly degenerate with the slope and amplitude of the primordial power spectrum. To see this quantitatively, we start with the line of sight solution to the temperature perturbation in direction $\hat{\mathbf{n}}$ [26],

$$\Delta(\hat{\mathbf{n}}) = \int_0^{\eta_0} \left[\dot{\tau} \left(\Psi + \frac{\Theta}{4} + \hat{\mathbf{n}} \cdot \mathbf{v}_b \right) + 2\dot{\phi} \right] e^{-\tau} \, d\eta \; , \quad (14)$$

where Ψ is the gravitational potential, Θ is the photon density perturbation, $\mathbf{v}_b$ is the baryon velocity, and we ignore vector and tensor contributions. If we ignore the

ISW [27] contribution $(2\dot{\phi})$ to the anisotropy spectrum, we obtain a useful semi-analytic approximation to the anisotropy spectrum by separating into slowly varying (potentials, $T(k)$ below) and rapidly varying (recombination, Silk damping, $D(k)$ below) terms [26],

$$C_l = 4\pi A \int_0^\infty d(\ln k) \, k^{n_s} D^2(k) T^2(k) \; , \quad (15)$$

implicitly assuming that $T^2(k)$ is evaluated at the redshift of last scattering and has no time dependence. The damping function is given by [28],

$$D(k) = \int dz \, g(z) \exp\left(-\frac{k^2}{k_D^2(z)} \right) \; , \quad (16)$$

where $g(z)$ is the visibility function introduced earlier, and k_D is the Silk damping scale given by [29],

$$\frac{1}{k_D^2} = \int_z^\infty dz \, \frac{c}{H^2(z)} \frac{1}{6(1+R)\tau'(z)} \left[\frac{R^2}{(1+R)} + \frac{16}{15} \right] \; , \quad (17)$$

where $R = 3\rho_b/4\rho_\gamma$ is the baryon-photon ratio. Since the ionization history only appears in Eq. 15 through the optical depth in $D(k)$, we estimate the effect of adding an ionization floor by computing $D(k)/D_0(k)$, where $D_0(k)$ assumes the standard ionization history.

As the relevant regime is when the ionization fraction is rapidly changing, we numerically integrate Eq. 16 and compute $D(k)/D_0(k)$ for different $\epsilon_{dm,0}$. The results for our fiducial cosmology are shown in Fig. 5. The scales relevant for $l > 50$ in the CMB correspond approximately to $k > 0.001 h\text{Mpc}^{-1}$; Fig. 5 demonstrates that $D(k)/D_0(k)$ is remarkably well described by a power law, $k^{-\alpha}$, over these scales. This signals a near exact degeneracy in the CMB; examining Eq. 15 suggests that the effect of the ionization floor can be almost exactly compensated by adjusting $n_s \to n_s + 2\alpha$, and changing the amplitude, A. The residual differences can be corrected by adjusting (at sub-percent levels) the remaining cosmological parameters.

We emphasize that this degeneracy appears to be purely accidental. As $k \to 0$, Silk damping becomes increasingly unimportant and $D(k)/D_0(k) \to 1$. In addition, we have ignored the ISW contribution, which has a different visibility function, and therefore will not be compensated by changing the scalar spectral index. On small scales ($k \to \infty$) that are considerably damped before recombination, the correction to the visibility function due to the ionization floor is negligible and again, one would expect $D(k)/D_0(k) \sim$ constant. These two limits are however hard to constrain, large scales because of cosmic variance, and small scales because of secondary anisotropies. On intermediate scales where high S/N measurements of CMB can be made, the effect of an ionization floor is degenerate with changing the scalar spectral index.

Estimating the effect of ϵ_{dm} on the polarization of the CMB is more involved. Polarization principally results
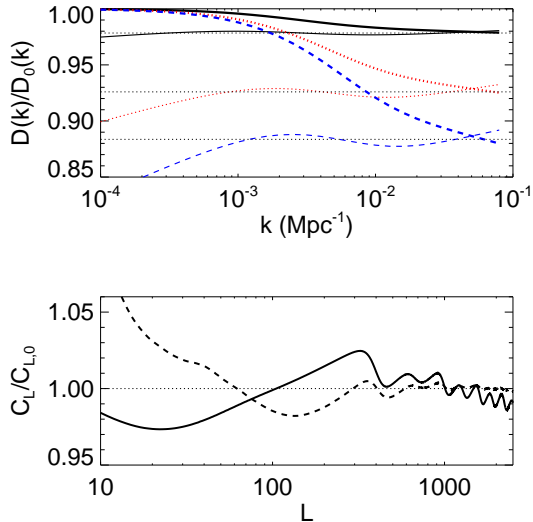
FIG. 5: (Top) The heavy lines show the ratio of damping functions $D(k)/D_0(k)$ for $\epsilon_{dm,0}$ of 100, (solid), 500 (dotted), and 1000×10^{-25}eV/s (dashed) and our fiducial cosmology. The light lines show this same ratio divided by $(k/k_{fid})^{-\alpha}$ where $k_{fid} = 0.05$ Mpc^{-1}. The horizontal dotted lines are a visual guide. (Bottom) The solid line shows the ratio of a model with no DM annihilation, but with n_s altered using the analytic calculation above, to our fiducial model with $\epsilon_{dm,0} = 500 \times 10^{-25}$eV/s. The dashed line has the same ratio, except that all the cosmological parameters are adjusted to best fit the model with DM annihilation.

from the Thomson scattering of the local quadrupole in the temperature distribution. However, the quadrupole vanishes during the tightly coupled regime before recombination; the only source of a quadrupole is the free streaming of the monopole and dipole perturbations during recombination. Ignoring the effects of reionization, the amplitude of the quadrupole contributing to polarization can be schematically written as [30],

$$\Theta_2(k) \sim \Theta_0(k)j_2(x) + 3\Theta_1(k)\left[j_1(x) - \frac{3j_2(x)}{x}\right] \quad (18)$$

where Θ_l with $l = 0, 1, 2$ represents the monopole, dipole and quadrupole components of photon distribution, and $x = k\Delta\eta$, where $\Delta\eta$ is the thickness of the last scattering surface. Focusing on scales much larger than the thickness of the last scattering surface, $x \ll 1$, we obtain,

$$\Theta_2(k) \sim \frac{\Theta_0(k)[k\Delta\eta]^2 + 6\Theta_1[k\Delta\eta]}{15} + \mathcal{O}(x^3) , \quad (19)$$

where we used the expansion $j_l(x) = x^l/(2l + 1)!! + \mathcal{O}(x^{l+2})$. Increasing the width of the last scattering surface therefore increases the amplitude of the polarization fluctuations. Furthermore, Eq. 19 implies that the quadrupole is dominated by free-streaming from the dipole perturbations. These are $\pi/2$ out of phase with

the monopole, resulting in the well known phase structure of the CMB temperature and polarization spectrum peaks. As the last scattering surface grows thicker, the fractional contribution from monopole perturbations to the quadrupole increases, shifting the positions of the TE and EE peaks. Finally, on smaller scales, the TE and EE power spectra are attenuated by increased scattering, analogous to the TT power spectrum. These trends are seen in the TE and EE power spectra in Fig. 4.

IV. ESTIMATING DETECTABILITY

A. Formalism

Given a measurement of the CMB sky with detector noise and cosmic variance, how distinguishable are any two models? And does there exist a combination of standard CMB parameters that can mimic DM annihilation? To answer the first question, we assume a realization of the full sky both in temperature and polarization (E modes). The likelihood of observing these maps is,

$$\mathcal{L}(\mathbf{d}|\text{theory}) \propto \frac{1}{\sqrt{\det \mathbf{C}}} \exp\left(-\frac{1}{2}\mathbf{d}^t\mathbf{C}^{-1}\mathbf{d}\right) , \quad (20)$$

where we have assembled the maps into the vector $\mathbf{d}$, and the covariance matrix, $\mathbf{C}$, is a function of the theoretical model. We transform to the spherical harmonic basis,

$$\mathcal{L}(\mathbf{d}|\text{theory}) \propto \prod_{l,m} \frac{1}{\sqrt{\det \mathbf{C}_l}} \exp\left(-\frac{1}{2}\mathbf{d}_{lm}^t\mathbf{C}_l^{-1}\mathbf{d}_{lm}\right) , \quad (21)$$

where $\mathbf{d}_{lm}^t = (a_{lm}^T, a_{lm}^E)$ is the spherical transform of the temperature and E-mode maps respectively. The 2×2 covariance matrix for each l, m mode is given by

$$\mathbf{C}_l = \begin{pmatrix} C_l^{TT} & C_l^{TE} \\ C_l^{TE} & C_l^{EE} \end{pmatrix} , \quad (22)$$

where C^{TT}, C^{EE}, and C^{TE} are the temperature and E-mode angular auto-power spectra and cross-power spectrum respectively. Taking logarithms and summing over azimuthal modes, we get

$$\log[\mathcal{L}(d|C)] = -\frac{1}{2}\sum_l(2l+1)\left[\log(\det \mathbf{C})+\right.$$
$$\left.\frac{C^{TT}\hat{C}^{EE} + C^{EE}\hat{C}^{TT} - 2C^{TE}\hat{C}^{TE}}{\det \mathbf{C}}\right] , \quad (23)$$

where $\det \mathbf{C} = C^{TT}C^{EE} - (C^{TE})^2$, the hat denotes observed quantities, and the l dependence is suppressed.

We can now compare the likelihoods for two different theoretical models, $\mathbf{C}$ and $\mathbf{C}'$,

$$r \equiv \log\left(\frac{\mathcal{L}(d|\mathbf{C})}{\mathcal{L}(d|\mathbf{C}')}\right) , \quad (24)$$

obtaining

$$r = -\frac{1}{2}\sum_l (2l+1)\left[\log\left(\frac{\det \mathbf{C}}{\det \mathbf{C}'}\right) + \right.$$
$$\left. \alpha\hat{C}^{TT} + \beta\hat{C}^{EE} + \gamma\hat{C}^{TE}\right] , \qquad (25)$$

where

$$\alpha = \left(\frac{C^{EE}}{\det \mathbf{C}} - \frac{C^{EE'}}{\det \mathbf{C}'}\right) , \qquad (26)$$

$$\beta = \left(\frac{C^{TT}}{\det \mathbf{C}} - \frac{C^{TT'}}{\det \mathbf{C}'}\right) , \qquad (27)$$

$$\gamma = -2\left(\frac{C^{TE}}{\det \mathbf{C}} - \frac{C^{TE'}}{\det \mathbf{C}'}\right) . \qquad (28)$$

If we assume that the data is a realization of $\mathbf{C}$, we have a simple criterion for distinguishability (and therefore, detectability) – two models are distinguishable if the probability that $r < 0$, $P(r < 0)$, is less than a chosen threshold (the confidence level). To compute $P(r < 0)$, we compute

$$\langle r\rangle = -\frac{1}{2}\sum_l (2l+1)\left[\log\left(\frac{\det \mathbf{C}}{\det \mathbf{C}'}\right) + \right.$$
$$\left. \alpha C^{TT} + \beta C^{EE} + \gamma C^{TE}\right] , \qquad (29)$$

and

$$\mathrm{Var}(r) = \frac{1}{2}\sum_l (2l+1)\left[\alpha^2(C^{TT})^2 + \beta^2(C^{EE})^2 + \right.$$
$$\frac{\gamma^2}{2}[(C^{TE})^2 + C^{EE}C^{TT}] + 2\alpha\beta(C^{TE})^2 +$$
$$\left. + 2\beta\gamma C^{TE}C^{EE} + 2\alpha\gamma C^{TE}C^{TT}\right] \approx 2\langle r\rangle , \ (30)$$

where we use standard contraction formulae to compute the four point functions, and the last approximation is good when $\mathbf{C}$ is very close to $\mathbf{C}'$. The central limit theorem ensures that the distribution of r is well approximated by a Gaussian; we therefore obtain,

$$P(r < 0) = \frac{1}{2}\left[1 - \mathrm{erf}\left(\frac{\langle r\rangle}{\sqrt{2\mathrm{Var}(r)}}\right)\right] . \qquad (31)$$

The above expressions can be generalized to take into account of detector noise; one substitutes $C^x \rightarrow C^x + N^x$, where $x = TT, EE$ assuming the temperature and polarization measurements are uncorrelated. The noise is determined by the angular size of the telescope beam, and the temperature sensitivity of the detectors [31, 32],

$$N(l) = (w_p)^{-1}\exp\left[l(l+1)\theta^2\right] , \qquad (32)$$

where θ is related to the FWHM of the beam by FWHM $= \theta\sqrt{8\ln 2}$, $(w_p)^{-1/2} = \Delta T \times$ FWHM, and all angles are in radians.

We now state our algorithm for the detectability of DM annihilation:

Experiment	Beam FWHM (arcmin)	$10^6\Delta T/T$ (I)	$10^6\Delta T/T$ (Q,U)
WMAP (V band)	21	11.0	15.6
Planck (143 Ghz)	7.1	2.2	4.2
HiRes POL	3.0	1.0	1.0
Cosmic Variance	0.0	0.0	0.0

TABLE I: Detector sensitivities and beams for different CMB temperature and polarization experiments. HiRes POL refers to a hypothetical all sky CMB polarization experiment.

Experiment	$\epsilon_{dm,0}(10^{-25}$ eV/s)		
	68%	90%	99%
WMAP (V band)	1.5e2	5.6e2	1.1e3
Planck (143 Ghz)	1.1e1	3.2e1	6.2e1
HiRes POL	4.1	1.2e1	2.2e1
Cosmic Variance	4.0	1.1e1	2.1e1

TABLE II: Detectable values of ϵ_{dm} at 68%, 90%, and 99% confidence levels, for different experimental parameters (Table I).

1. Consider two cosmological models, one with $\epsilon_{dm} = 0$ and the other with $\epsilon_{dm} > 0$. For simplicity, we assume a minimal cosmological model with 6 parameters (Ω_M, Ω_b, h, n_s, A, τ).

2. We adjust these parameters for the model with no DM annihilation to minimize $\langle r\rangle$.

3. At the minimum, we compute $\mathrm{Var}(r)$ and $P(r < 0)$, thereby obtaining a measure of the detectability of ϵ_{dm}.

This algorithm is complementary to the Fisher information methods currently popular in cosmology. The Fisher information probes the likelihood function in the neighborhood of a fiducial point, estimating the minimal theoretically achievable errors. On the other hand, we explicitly track the degeneracy locus well beyond the immediate neighborhood of a fiducial model.

B. Results

We consider four different experiments - a cosmic variance limited experiment, a hypothetical high resolution polarization experiment (hereafter HiRes POL), the *Planck* 143 Ghz channel [46] and the *WMAP* V band [32][47]. The parameters chosen for HiRes POL are similar to those projected for (eg. NASA's CMBpol [48]) missions designed to detect the imprint of gravitational radiation from inflation. The assumed noise and beam characteristics of these experiments are in Table I, and the noise power spectra are plotted in Fig. 4. Note that our aim here is to consider representative parameters, and not an optimization of experimental specifications.

The results are summarized in Fig. 6 and Table II. A principal feature is the significant improvement of *Planck* over *WMAP* , due to the introduction of high S/N
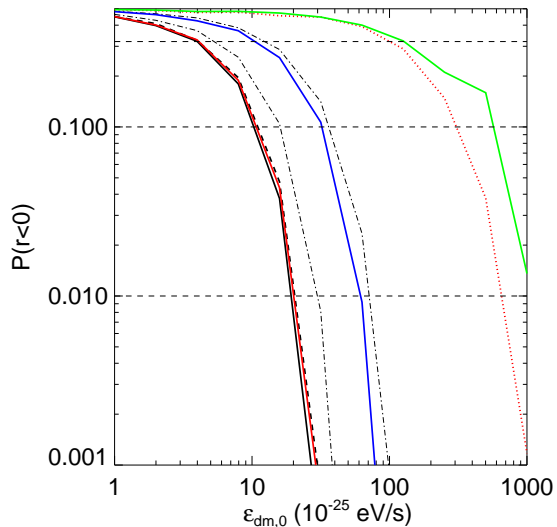
FIG. 6: The detectability of a given injection energy, $\epsilon_{dm,0}$, for the different experimental specifications of Table I, assuming a maximum multipole, $l_{max} = 2500$. The lines, from left to right, are for cosmic variance, HiRes POL, the *Planck* 143 Ghz channel, and the *WMAP* V band. The dashed line shows the cosmic variance detectability for $l_{max} = 1500$, while the dot-dashed lines show it for 20% and 50% sky coverage. The dotted line uses the parameters for HiRes POL, but with no polarization information. Also shown are the 68%, 90%, and 99% levels.
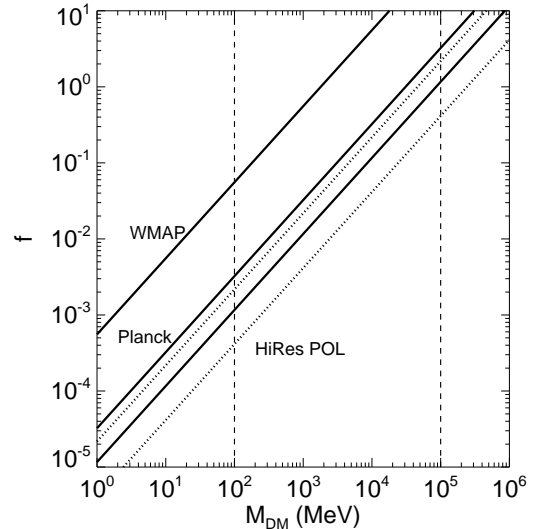
FIG. 7: The 90% exclusion region in the $M_{DM} - f$ plane, for (from top to bottom) *WMAP* , *Planck* and HiRes POL; regions above the lines can be excluded by these experiments. This assumes our fiducial cosmology, and Eq. 6 to relate f and M_{DM} to ϵ_{dm}; $\langle \sigma_A v \rangle$ is set to the value required for a thermal relic density, but deviations from this can be absorbed into f. The dotted lines also show the 68% and 99% exclusion regions for our hypothetical polarization experiment.

polarization data, evident in Fig. 4. The importance of polarization is further emphasized by comparing HiRes POL, to an experiment with the same temperature but no polarization sensitivity. As discussed earlier, the temperature power spectrum suffers from a degeneracy between n_s and ϵ_{dm}, and therefore cannot constrain ϵ_{dm} by itself. Introducing polarization breaks this degeneracy, allowing ϵ_{dm} to be measured with significantly greater sensitivity. We also observe that HiRes POL (almost) achieves the cosmic variance sensitivity limits.

The advantage of phrasing the limits in terms of $\epsilon_{dm,0}$ is that they are independent of a particular DM model, or indeed, of any mechanism for the injection of additional energy during recombination. However, for a single species of DM, Eq. 5 relates M_{DM}, Ω_{DM}, $\langle \sigma_A v \rangle$ and f to $\epsilon_{dm,0}$. Furthermore, f and $\langle \sigma_A v \rangle$ are degenerate with each other, allowing us to translate our limits on ϵ_{dm} into constraints in the f-M_{DM} plane. Fig. 7 does this for our fiducial cosmological model, using Eq. 6 and Table II. We observe that, assuming $f \sim 0.1 - 1$, *Planck* will be able to detect (at 90% confidence) DM annihilation from particles with masses less than $\sim 3 - 30$ GeV, while HiRes POL increases that lower bound to $\sim 10 - 100$ GeV. These limits assume $\langle \sigma_A v \rangle = 2 \times 10^{-26}$ cm^3/s, appropriate for a thermal relic; a higher $\langle \sigma_A v \rangle$ (due to eg. co-annihilations) would proportionally increase the limits. We note that these limits probe relevant parts of its.

parameter space, and are complementary to accelerator and direct detections, since they make very different assumptions.

It is timely to ask what parts of DM model space can be constrained by *WMAP* . Fig. 7 shows that *WMAP* will have no sensitivity to DM models with masses > 1 GeV, and therefore, to the traditional DM candidates. However, [33, 34, 35] have proposed a light ($\sim 10 - 100$ MeV) DM particle to explain the 511 keV flux observed by the INTEGRAL satellite. Since the particle mass is below the photon transparency window, the annihilation energy is efficiently converted into ionizations, suggesting that such models will be strongly constrained by the *WMAP* polarization measurements.

The discussion above focuses on the detection of an unknown particle, and we therefore have concentrated on the simplest case of a single species of DM. Reality could well be more complicated, and the DM could well consist of multiple species. In such a case, in addition to determining the nature of the DM, we would need to determine the relative contribution of the different species. Given a particle with a known mass and annihilation cross section, constraints on ϵ_{dm} put an upper bound on the density of these particles, without making any assumptions about whether the particle is a thermal relic or not. Fig. 8 demonstrates this for different values of M_{dm}, $\langle \sigma_A v \rangle$ and f. This emphasizes the complementary nature of astrophysical and particle physics probes of DM; at low masses, the CMB is competitive with di-
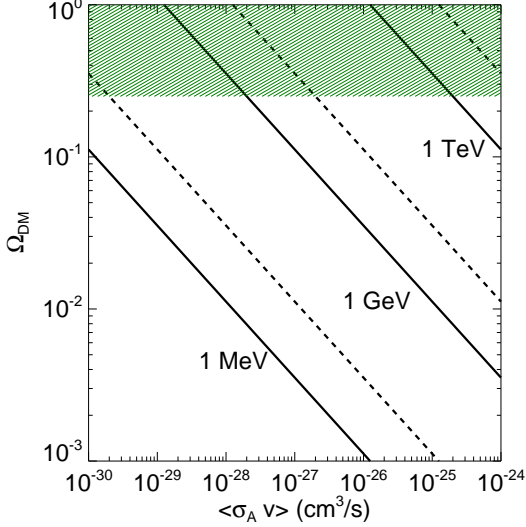
FIG. 8: Contours in the Ω_{DM}-$\langle\sigma_A v\rangle$ plane with $\epsilon_{dm,0} = 10^{-24}$ eV/s, for $M_{DM}/f = 1$ TeV, 1 GeV, and 1 MeV (solid), and 10 TeV, 10 GeV, and 10 MeV (dashed). Regions above these contours are accessible to an experiment with the sensitivity to measure $\epsilon_{dm,0} = 10^{-24}$ eV/s. The shaded region shows the region excluded by our fiducial model.

rect detection and accelerator searches of DM. However, given a detected DM particle, the CMB probes, with minimal assumptions, its cosmological density, that in turn, has the potential to constrain theoretical models for its formation.

V. OTHER ASTROPHYSICAL CONSTRAINTS

Does DM annihilation during the recombination epoch have other observational consequences? We consider three possibilities - distortions to the CMB spectrum, redshifted photons contributing to the diffuse photon background, and molecular hydrogen production.

We start by considering the additional energy density injected per unit time at $z = 1000$ due to DM annihilation,

$$
\begin{aligned}
\mathcal{E} &= \langle\sigma_A v\rangle M_{DM} n_{DM}^2 \\
&\sim 2 \times 10^{-13} \text{ eV/cm}^3/\text{s} \left(\frac{1+z}{1000}\right)^6 \times \\
&\left(\frac{\Omega_{DM}h^2}{0.12}\right)^2 \left(\frac{\langle\sigma_A v\rangle}{2 \times 10^{-26} \text{ cm}^3/\text{s}} \frac{100 \text{ GeV}}{M_{DM}}\right) .(33)
\end{aligned}
$$

Over a Hubble time, the energy injected is

$$
\begin{aligned}
E &\sim 2 \text{ eV/cm}^3 \left(\frac{1+z}{1000}\right)^{9/2} \left(\frac{0.147}{\Omega_M h^2}\right)^{1/2} \times \\
&\left(\frac{\Omega_{DM}h^2}{0.12}\right)^2 \left(\frac{\langle\sigma_A v\rangle}{2 \times 10^{-26} \text{ cm}^3/\text{s}} \frac{100 \text{ GeV}}{M_{DM}}\right) .(34)
\end{aligned}
$$

This is much less than the energy density of the CMB,

$$
E_{CMB} \sim 0.25 \times 10^{12} \left(\frac{1+z}{1000}\right)^4 \text{ eV/cm}^3 , \quad (35)
$$

implying that the distortions are below detection thresholds. We also note that although during matter domination, the energy from DM annihilation is growing faster than the CMB energy density, the exponent of $9/2$ changes to 4 during radiation domination, and so the injected energy density from DM annihilation never is a substantial fraction of the CMB energy density.

Could photons from DM annihilations, injected into an optically thin part of the spectrum, be detected as part of the diffuse photon background today? The transparency region from 10^8 to 10^{10} eV in Fig. 1 implies that these photons would have energies between 10^5 and 10^7 eV today. Furthermore, Eq. 34 for standard parameters gives a present-day photon energy density of $E \sim 2 \times 10^{-12}$ eV/cm^3, implying a flux of 0.5×10^{-2} eV/cm^2/s/sr. Comparing this to the observed flux of 1×10^3 eV/cm^2/s/sr [36, 37, 38], we find that the fraction possibly due to DM annihilation is considerably below the uncertainties in the measurement.

The residual ionization after recombination serves as a catalyst for the production of molecular hydrogen, first via $2H + H^+ \rightarrow H_2 + H^+$ at $z \sim 500$, and then by $2H + e^- \rightarrow H_2 + e^-$ at $z \sim 100$. Molecular hydrogen is important since it serves as a coolant, allowing for the collapse of the first cosmological objects. A higher ionization fraction could, in principle, create a greater abundance of molecular hydrogen, triggering collapse at an earlier epoch. The equation for the evolution of the molecular hydrogen fraction, $f \equiv n[H_2]/n[H]$, is [39]

$$
H(a)\frac{df}{d\ln a} = k_{eff}(1 - x - 2f)nx , \quad (36)
$$

where x is the ionization fraction and $n = n[H]+n[H^+]+n[H_2]$ is the density of hydrogen atoms, and k_{eff} is the effective rate coefficient, approximately constant for $x, f \ll 1$. For $x \ll 1$, Eq. 36 describes a catalyst-starved reaction; increasing x proportionally increases the H_2 fraction. The standard recombination scenario produces an H_2 fraction of $\sim 10^{-6}$ [40] However, the fraction required to efficiently cool halos is approximately 10^{-3}; primordial H_2, even with an enhanced ionization fraction, is too small to significantly alter structure formation. The required H_2 is produced in regions of high density, where the reaction rates are significantly higher. Unfortunately, this process is relatively insensitive to initial conditions [39], making it difficult to constrain the H_2 and ionization fractions.

VI. DISCUSSION

We have considered the effect that DM annihilation has on the recombination history of the universe, and therefore, on the CMB temperature and polarization power

spectra. We argued that the effect of DM annihilation on the IGM is well approximated by an injection of a fraction f of the rest mass energy of the DM particles into the IGM, where it is instantaneously used to heat and ionize the IGM. This "on the spot" approximation allowed us to compute the altered recombination history; the epoch of recombination is unchanged, but the residual ionization fraction increases. This broadens the visibility function, suppressing the temperature power spectrum, but enhancing the polarization power spectrum. Furthermore, the thicker visibility function shifts the peaks in TE and EE power spectra relative to the peaks in the TT power spectrum.

Given the modified power spectra, we can ask whether the changes are detectable, or if they are degenerate with other cosmological parameters? A cosmic variance limited survey is sensitive to an energy injection rate of $\epsilon_{dm,0} \sim 10^{-24}$ eV/s, probing masses $\lesssim 100$ GeV. Furthermore, these limits are attainable by CMB experiments designed to detect the polarization created by the stochastic gravitational wave background. The limits for *Planck* are about an order of magnitude worse, and the limits are significantly degraded for *WMAP* , due to its polarization sensitivity. However, *WMAP* will be able to constrain low mass ($\mathcal{O}(10$ MeV -1 GeV$)$) DM particles such as those proposed by [35].

We have kept our analysis as generic and idealized as possible, to ensure that our results are independent of the particulars of any DM model. We now consider some of the issues ignored by the analysis above.

- *How does one calculate f?* In order for a DM model to make a falsifiable prediction, it is important to be able to calculate f for a given model. A simple algorithm to compute f given all the decay channels and their branching ratios (admittedly a tedious task!) is :

  - Compute the $e^{\pm}$ and photon energy spectra resulting from an annihilation.
  - Evolve the photon and $e^{\pm}$ spectra with the processes in Fig. 2.
  - Redshift the spectra to the next time and repeat.

  One can obtain a qualitative picture of the results by considering Fig. 1. For photons below $\sim 10^8$ eV and electrons below 10^{10} eV, the energy is efficiently deposited ($\sim 0.1 - 1$) into the IGM. At higher energies, the efficiency is dictated by efficiency of pair production; however, even in this case, one would expect a non-negligible ($\sim 0.01 - 0.1$) fraction to be converted into ionizations and heat. One consequence is that one would expect f to generically increase with decreasing mass, weakening our ability to constrain the highest masses but strengthening constraints on lower masses. Finally, to compare to plots such as Fig. 7, one must also include variations in $\langle \sigma_A v \rangle$ in f.

While $\langle \sigma_A v \rangle$ is only logarithmically dependent on M_{DM} for a thermal relic density of a single species, it can vary significantly if one includes the possibilities of multiple DM species or co-annihilations. Just how generic these processes are will depend on the class of theories being considered; initial attempts to answer such questions within the framework of the MSSM are in [41].

- *Is the standard recombination calculation accurate enough?* Detecting DM annihilation by its effect on the recombination history requires that we understand the fiducial recombination physics to better than 1%. The current recombination calculation is accurate to $\sim 1\%$ [42], although there recently have been claims of corrections due to two photon processes[43]. Although the current calculation may not be accurate enough, we do not know of any theoretical limit that would prevent reaching the required accuracy. We should also emphasize that this accuracy is only necessary for detecting injection energies $\sim 10^{-25}$ eV/s; the current calculation is accurate enough to detect higher energies.

- *What about real-world complications?* The limits on DM annihilation projected in Sec. IV assumed an idealized CMB experiment with full sky coverage, and no contamination to the primary CMB due to Galactic and extragalactic foregrounds. We briefly discuss these below; we however emphasize that these are not complications peculiar to measuring DM annihilation, but will affect any high precision polarization experiment (eg. detecting the gravitational wave background in the CMB).

  Decreasing the sky coverage reduces the number of available modes, increasing the errors due to cosmic variance and degrading our ability to distinguish between models. A full sky CMB experiment at these sensitivities might survey an effective sky fraction of 50% due to Galactic and point source cuts, increasing the errors by $\sqrt{2}$; the impact of which is shown in Fig. 6. Even after excluding the most contaminated regions of the mask, it will be necessary to separate Galactic and extragalactic foregrounds using their frequency dependence. This problem has been examined in detail by a number of authors [eg. 32], who demonstrate that this separation is possible on large angular scales. Furthermore, extragalactic foregrounds start to dominate only on small angular scales ($l \sim 2500$), while the signal from DM annihilation is maximal on larger scales $l < 1500$ (Fig. 6), suggesting that foregrounds are a tractable problem.

We conclude by reiterating the complementarity between the different probes of DM. As seen above, the CMB is able to put strong constraints on the cosmological abundance of a light ($\ll 100$ GeV) DM particle that evades accelerator searches. At higher masses

(> 100 GeV), the injected energy from annihilations decreases and the CMB is no longer competitive with other searches. However, given a DM candidate with a known mass and annihilation cross section, the injection energy constraints from the CMB translate into a constraint on the density of these particles. Importantly, this does not assume that the particle is a thermal relic, allowing us to constrain the particle content of the DM, including particles that produced via non-equilibrium processes.

Understanding the properties of the dark matter remains one of the most important problems in cosmology today. And astrophysical probes, such as the one discussed here, have an important role to play, both in detecting possible candidates and understanding their cosmological abundance.

[1] G. Jungman, M. Kamionkowski, and K. Griest, Physics Reports **267**, 195 (1996).
[2] G. Bertone, D. Hooper, and J. Silk, Physics Reports **405**, 279 (2004).
[3] C. L. Bennett, M. Bay, M. Halpern, G. Hinshaw, C. Jackson, N. Jarosik, A. Kogut, M. Limon, S. S. Meyer, L. Page, et al., Astrophys. J. **583**, 1 (2003).
[4] D. S. Akerib, J. Alvaro-Dean, M. S. Armel-Funkhouser, M. J. Attisha, L. Baudis, D. A. Bauer, J. Beaty, P. L. Brink, R. Bunker, S. P. Burke, et al., Physical Review Letters **93**, 211301 (2004).
[5] S. D. Hunter, D. L. Bertsch, J. R. Catelli, T. M. Dame, S. W. Digel, B. L. Dingus, J. A. Esposito, C. E. Fichtel, R. C. Hartman, G. Kanbach, et al., Astrophys. J. **481**, 205 (1997).
[6] A. W. Strong, I. V. Moskalenko, and O. Reimer, Astrophys. J. **537**, 763 (2000).
[7] W. de Boer, Fifth International Heidelberg Conference on Dark Matter In Astro And Particle Physics (2004), astro-ph/0412620.
[8] B. J. Teegarden, K. Watanabe, P. Jean, J. Knodlseder, V. Lonjou, J. P. Roques, G. K. Skinner, P. von Ballmoos, G. Weidenspointner, A. Bazzano, et al., Astrophys. J. accepted (2004), astro-ph/0410354.
[9] J. J. Beatty, A. Bhattacharyya, C. Bower, S. Coutu, M. A. Duvernois, S. McKee, S. A. Minnick, D. Müller, J. Musser, S. Nutter, et al., Physical Review Letters **93**, 241102 (2004).
[10] D. P. Finkbeiner, Astrophys. J. **614**, 186 (2004).
[11] E. A. Baltz and L. Wai, Phys. Rev. D **70**, 023512 (2004).
[12] J. F. Navarro, C. S. Frenk, and S. D. M. White, Astrophys. J. **490**, 493 (1997).
[13] D. P. Finkbeiner, Astrophys. J. submitted (2004), astro-ph/0409027.
[14] X. Chen and M. Kamionkowski, Phys. Rev. D **70**, 043502 (2004).
[15] P. J. E. Peebles, S. Seager, and W. Hu, Astrophys. J. Lett. **539**, L1 (2000).
[16] R. Bean, A. Melchiorri, and J. Silk, Phys. Rev. D **68**, 083501 (2003).
[17] S. H. Hansen and Z. Haiman, Astrophys. J. **600**, 26 (2004).
[18] E. Pierpaoli, Physical Review Letters **92**, 031301 (2004).

[19] A. G. Doroshkevich, I. P. Naselsky, P. D. Naselsky, and I. D. Novikov, Astrophys. J. **586**, 709 (2003).
[20] A. A. Zdziarski and R. Svensson, Astrophys. J. **344**, 551 (1989).
[21] R. Svensson and A. Zdziarski, Astrophys. J. **349**, 415 (1990).
[22] G. R. Blumenthal and R. J. Gould, Reviews of Modern Physics **42**, 237 (1970).
[23] J. M. Shull and M. E. van Steenberg, Astrophys. J. **298**, 268 (1985).
[24] S. Seager, D. D. Sasselov, and D. Scott, Astrophys. J. Lett. **523**, L1 (1999).
[25] A. Lewis, A. Challinor, and A. Lasenby, Astrophys. J. **538**, 473 (2000).
[26] U. Seljak, Astrophys. J. Lett. **435**, L87 (1994).
[27] R. K. Sachs and A. M. Wolfe, Astrophys. J. **147**, 73 (1967).
[28] W. Hu and N. Sugiyama, Astrophys. J. **444**, 489 (1995).
[29] M. Zaldarriaga and D. D. Harari, Phys. Rev. D **52**, 3276 (1995).
[30] S. Dodelson, *Modern cosmology* (Academic Press, Amsterdam (Netherlands), 2003).
[31] L. Knox, Phys. Rev. D **52**, 4307 (1995).
[32] M. Tegmark, D. J. Eisenstein, W. Hu, and A. de Oliveira-Costa, Astrophys. J. **530**, 133 (2000).
[33] C. Bœhm and P. Fayet, Nuclear Physics B **683**, 219 (2004).
[34] C. Bœhm, P. Fayet, and J. Silk, Phys. Rev. D **69**, 101302 (2004).
[35] C. Boehm, D. Hooper, J. Silk, M. Casse, and J. Paul, Physical Review Letters **92**, 101301 (2004).
[36] P. Sreekumar, D. L. Bertsch, B. L. Dingus, J. A. Esposito, C. E. Fichtel, R. C. Hartman, S. D. Hunter, G. Kanbach, D. A. Kniffen, Y. C. Lin, et al., Astrophys. J. **494**, 523 (1998).
[37] G. Weidenspointner, M. Varendorff, S. C. Kappadath, K. Bennett, H. Bloemen, R. Diehl, W. Hermsen, G. G. Lichti, J. Ryan, and V. Schöfelder, in *American Institute of Physics Conference Series* (2000).
[38] A. W. Strong, I. V. Moskalenko, and O. Reimer, Astrophys. J. **613**, 956 (2004).
[39] M. Tegmark, J. Silk, M. J. Rees, A. Blanchard, T. Abel, and F. Palla, Astrophys. J. **474**, 1 (1997).

[40] D. Galli and F. Palla, Astron. Astrophys. **335**, 403 (1998).

[41] E. A. Baltz and P. Gondolo, Journal of High Energy Physics **10**, 52 (2004).

[42] S. Seager, D. D. Sasselov, and D. Scott, Astrophys. J. Supp. **128**, 407 (2000).

[43] V. K. Dubrovich and S. I. Grachev, Astronomy Lett. accepted (2005), astro-ph/0501672.

[44] The use of "Inter-Galactic Medium" for the photon-baryon fluid at $z \sim 1000$ is a convenient anachronism; we use it throughout without further apology.

[45] Positrons behave identically to electrons at high energies, while at low energies, they annihilate releasing 2×511 keV in photons.

[46] http://www.esa.int/science/planck

[47] http://lambda.gsfc.nasa.gov

[48] Now designated as the "Inflation Probe".

[49] http://idlastro.gsfc.nasa.gov/